22. Gas Hydrate and Free Gas Saturations Estimated from Velocity Logs on Hydrate Ridge, Offshore Oregon, USA[1]

M.W. Lee[2] and T.S. Collett[2]

ABSTRACT

During Ocean Drilling Program Leg 204, nine sites were logged on the Oregon continental margin, where one of the objectives of the integrated downhole logging program was to determine the distribution and saturation of gas hydrates and free gas in an accretionary ridge and adjacent slope basin. Downhole logs measured at Sites 1244, 1245, and 1247, drilled on Hydrate Ridge, were analyzed to constrain the physical properties of in situ gas-hydrate-bearing sediments. Saturations of gas hydrate in pore space are estimated from shear-wave (S-wave) velocities using the modified Biot-Gassmann theory, referred to as the BGTL. The average gas hydrate saturations are 10%, 10%, and 6% for Site 1244 (76–127 meters below seafloor [mbsf]), Site 1245 (73–129 mbsf), and Site 1247 (74–129 mbsf), respectively, and are comparable to estimates from downhole electrical resistivity logs. Free gas saturations were also estimated from the Biot-Gassmann theory with parameters derived from the BGTL using compressional-wave (P-wave) velocities and from elastic moduli using both P- and S-wave velocities. The exact amount of free gas is difficult to determine because of the uncertainties associated with the mode of gas distribution (patchy or uniform), but both methods provide comparable estimates for free gas saturations. This study suggests that free gas coexists with gas hydrate in the gas hydrate stability zone at these sites. This is the first reported evidence for coexistence of gas hydrate and free gas away from the summit vents.

INTRODUCTION

The assessment of gas hydrate and free gas associated with the base of the gas hydrate stability zone (GHSZ), which often coincides with bottom-simulating reflections (BSRs), becomes important as methane gas stored in gas-hydrate-bearing sediments is recognized as a potential energy resource, a greenhouse gas, and a factor controlling seafloor stability (Dillon et al., 1991; Holbrook et al., 1996; Sloan et al., 1999).

Gas hydrate in sediments increases both *P*- and *S*-wave velocities. A small amount of gas in sediments greatly diminishes *P*-wave velocity, whereas *S*-wave velocity is insensitive to the presence of gas (Domenico, 1977; Murphy, 1984).

Gas hydrate has been quantified in drill sites using sonic and electrical resistivity logs (Collett, 1998; Guerin et al., 1999; Lee and Collett, 1999; Collett and Ladd, 2000; Lee, 2000). At the Ocean Drilling Program (ODP) Leg 164 drill sites, the estimated gas hydrate saturations within the gas hydrate occurrence zone from electrical resistivities are 3.3%, 5.2%, and 5.5% of the pore space at Sites 994, 995, and 997, respectively (Collett and Ladd, 2000). From the *P*-wave velocities and core porosities at the same sites on the Blake Ridge, estimations are 3.9%, 5.7%, and 3.8% for Sites 994, 995, and 997, respectively (Lee, 2000).

The amount of free gas below the BSRs has also been estimated from seismic *P*-wave velocities (Miller et al., 1991; Bangs et al., 1993; Katzman et al., 1994; Pecher et al., 1995; Holbrook et al., 1996) and from downhole logs (Guerin et al., 1999; Collett and Ladd, 2000). From the reduced *P*-wave velocities, Holbrook et al. (1996) showed that a conservative estimate of saturation of free gas trapped below the BSR at the Blake Outer Ridge is ~1% of porosity. Miller et al. (1991) used *P*-wave reflection coefficients, Pecher et al. (1995) used a full waveform inversion method, and Guerin et al. (1999) used elastic moduli of sediments to assess the amounts of gas in sediments. Because a small amount of gas alters the *P*-wave velocity dramatically and the reduction of *P*-wave velocity depends on how the gas is distributed in the pore space, a large degree of uncertainty exists in the estimations.

In order to better constrain in situ physical properties of gas-hydrate-bearing sediments and to calibrate the amount of gas hydrate or free gas estimated from geophysical remote sensing techniques on the southern part of Hydrate Ridge on the Cascadia accretionary margin offshore Oregon (USA), geophysical well logs, along with cores, were obtained during ODP Leg 204 in 2002. The purpose of this paper is to analyze some of the well logs from Sites 1244, 1245, and 1247 (Fig. F1) in order to estimate the amounts of in situ gas hydrate and fee gas.

Previously, gas hydrate on the Cascadia margin was recognized through the presence of a BSR on conventional multichannel seismic data (Davis and Hyndman, 1989), and the physical properties of gas-hydrate-bearing sediments were investigated from drill sites of ODP Leg 146 (Shipboard Scientific Party, 1994). Other geophysical investigations were conducted to better constrain the physical properties of gas-hydrate-bearing sediments (MacKay et al., 1994; Spence et al., 1995; Tréhu et al., 1995, 1999).

In this paper, the amount of gas hydrate in sediments on Hydrate Ridge is estimated by applying the modified Biot-Gassmann theory by Lee (BGTL) (Lee, 2002, 2003) to *S*-wave velocities. For the estimation of free gas, the classical Biot-Gassmann theory (BGT) with the Biot coefficient estimated from the BGTL is applied to the *P*-wave velocities. Satu-

F1. ODP Leg 204 site location map, p. 16.
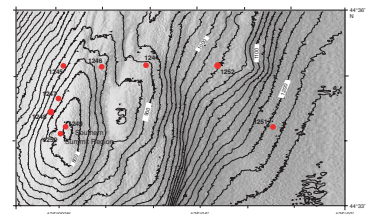
rations of gas hydrate estimated from velocity data are comparable to those estimated from electrical resistivity data. Also, saturations of free gas are comparable to those estimated from density and nuclear magnetic resonance (NMR) porosities.

THEORY

The effect of gas hydrate on velocities of unconsolidated sediments is modeled using the BGTL (Lee, 2002, 2003). The effect of free gas on velocities of unconsolidated sediments is modeled by the BGT with parameters derived from water-saturated sediments using the BGTL as demonstrated by Lee (2004). The difference between the BGT and BGTL is in the calculation of shear modulus of water-saturated sediments. This section summarizes the essence of the BGTL.

Elastic velocities (i.e., compressional velocity [V_P] and shear velocity [V_S]) of sediments can be computed from the elastic moduli using the following formulas:

$$V_P = \mathrm{SQR}[(k + 4\mu/3)/\rho]$$

and

$$V_S = \mathrm{SQR}(\mu/\rho), \qquad (1)$$

where

k = bulk modulus,
μ = shear modulus, and
ρ = density of the formation.

The formation density is given by

$$\rho = (1 - \phi)\rho_{ma} + \phi\rho_{fl}, \qquad (2)$$

where

ϕ = porosity,
ρ_{ma} = matrix density, and
ρ_{fl} = pore fluid density.

Under the low-frequency assumption, the bulk modulus of fluid-saturated sediment (k) is given by the following formula in terms of the Biot coefficient, β (Biot, 1941, 1956; Gassmann, 1951):

$$k = k_{ma}(1 - \beta) + \beta^2 M, \qquad (3)$$

where

$$1/M = [(\beta - \phi)/k_{ma}] + (\phi/k_{fl}), \qquad (4)$$

and

k_{ma} = bulk modulus of matrix, and
k_{fl} = bulk modulus of pore fluid.

The term $\beta^2 M$ represents the interaction of fluid filling the porosity with the solid skeleton of the formation, and the Biot coefficient measures the ratio of volume change of the fluid to the volume change of the formation (Krief et al., 1990).

If it is assumed that the velocity ratio, V_P/V_S, is constant irrespective of porosity and is equal to the velocity ratio of matrix, the shear modulus of dry rock (μ_d) is given by (Krief et al., 1990):

$$\mu_d = \mu_{ma} (1 - \beta), \tag{5}$$

where μ_{ma} is the shear modulus of the matrix. Conventionally, it is assumed that fluid in the pore space does not change the shear modulus of sediments. Therefore, the shear modulus of fluid-saturated sediment (μ) is the same as the dry shear modulus, (i.e., $\mu = \mu_d$), which is consistent with the BGT.

Lee (2004) derived the following shear modulus of water-saturated sediment assuming V_P/V_S is a function of porosity:

$$\mu_{bgtl} = [\mu_{ma}k_{ma}(1 - \beta)G^2(1 - \phi)^{2n} + \mu_{ma}\beta^2 MG^2(1 - \phi)^{2n}]/$$

$$\{k_{ma} + 4\mu_{ma}[1 - G^2(1 - \phi)^{2n}]/3\}, \tag{6}$$

where

μ_{bgtl} = the shear modulus calculated from equation 6, and
G, n = BGTL parameters.

As opposed to equation 5, the shear modulus predicted from the BGTL depends on the bulk modulus of fluid through M. Even though equation 5 is not the BGT (but is consistent with the BGT), Lee (2002) designated the use of equations 3 and 5 as the BGT to differentiate from the BGTL, which uses equations 3 and 6 to calculate elastic velocities.

For soft formations or unconsolidated sediments, the following Biot coefficient is used for the BGTL (Lee, 2002):

$$\beta = [-68.7421/(1 + e^{(\phi + 0.40635)/0.09425)}] + 0.98469. \tag{7}$$

As indicated in Lee (2004), the appropriate Biot coefficient for velocities of partially gas saturated sediments (β_{bgt}) is given by the following formula:

$$\beta_{bgt} = 1 - (\mu_{bgtl}/\mu_{ma}), \tag{8}$$

and in equations 3 through 5, β_{bgt} is substituted for β.

Two kinds of gas saturation in the pore space are considered: uniform and patch. Brie et al. (1995) suggested the following empirical mixing law based on the in situ downhole data:

$$k_{fl} = (k_w - k_g)S_w^e + k_g, \tag{9}$$

where

S_w = water saturation,
k_g = bulk modulus of gas, and
e = a calibration constant.

When e = 1, Brie et al.'s formula is the same as the isostrain (Voigt) average, proposed by Domenico (1977). As e increases, the patch saturation approaches the characteristics of uniform saturation and approaches nearly a uniform saturation at e = 40. Brie et al. (1995) showed that most downhole data they analyzed fit the mixing law with calibration constants between e = 2 and e = 5. However, other e values are appropriate depending on the frequency of measurement and the degree of consolidation.

In the BGTL formulation, two parameters are introduced to match the predicted velocity ratio with the measured velocity ratio or velocity. As shown in Lee (2003), these parameters are somewhat constrained by the nature of sediments, such as differential pressure, the degree of consolidation, and clay volume content. Lee (2003) suggested the following formula for n, based on laboratory data compiled by Prasad (2002):

$$n = [10^{(0.426 - 0.235 \log_{10} p)}]/m, \tag{10}$$

where

p = differential pressure in MPa, and
m = a parameter that depends on the degree of consolidation.

Usually, for unconsolidated sediments m varies from 1 to 2 and for consolidated sediments m varies from 4 to 5.

The scale G is introduced to compensate for the effect of clay or gas hydrate on the matrix material. Based on the data given by Han et al. (1986) and well logging data at the Mallik 5L-38 well, the following formula for G has been proposed (Lee, 2003; Lee and Collett, in press):

$$G = 0.9552 + 0.0448 e^{-C_v/0.06714} - 0.18 C_h^2, \tag{11}$$

where

C_v = the clay volume content, and
C_h = the saturation of gas hydrate in the pore space.

For a clean sandstone without gas hydrate, $G = 1$.

In summary, in the framework of BGTL, the parameter n is the only free parameter to choose, and it can be estimated by fitting the measured velocities to calculated velocities. G is an empirically derived parameter that depends on the clay volume content and gas hydrate saturations. The difference between the BGT and the BGTL is the method of calculating the shear modulus of the water-saturated sediments.

GEOLOGICAL SETTING

Hydrate Ridge is a 25-km-long and 15-km-wide ridge in the Cascadia accretionary complex, formed by the oblique subduction of Juan de Fuca plate beneath North America at a rate of ~4.5 cm/yr. Sediment on the subducting plate contains large volumes of sandy and silty turbidities (MacKay, 1995). It is characterized by a northern summit at a water depth of 600 m and a southern summit at a water depth of 800 m (Shipboard Scientific Party, 2003). As in many accretionary complexes, gas hydrate is present in this environment (Shipboard Scientific Party,

1994). Hydrate Ridge appears to be capped by hydrate, as indicated by a strong BSR (Tréhu et al., 1999) and by recovered samples of massive hydrate (Bohrmann et al., 1998).

Site 1244 is located in ~890 m of water in the eastern flank of Hydrate Ridge ~3 km northwest of the southern summit (Fig. F1), and a BSR is present at a depth of 124 mbsf. Site 1245 is located in 870 m of water on the western flank of Hydrate Ridge ~3 km northwest of the southern summit, and a BSR is present at a depth of ~134 mbsf. Site 1247 is located in 845 m of water on the western flank of Hydrate Ridge, and a BSR is present at ~121–124 mbsf. All three sites are well within the GHSZ (Shipboard Scientific Party, 2003). Unlike the summit region, there is no evidence of venting of bubbles at the seafloor at these sites.

DOWNHOLE LOGS

During Leg 204, conventional downhole wireline logs (CWL) and logging while drilling (LWD) logs were acquired (Shipboard Scientific Party, 2003). The logs are not necessary obtained from the same hole; however, the holes are always very close to each other and the best quality logs from the various holes were used for the analysis. The logs used in this analysis include density, P-wave velocity, S-wave velocity, natural gamma ray, electrical resistivity, and NMR logs acquired at Sites 1244, 1245, and 1247 (Holes 1244E, 1245E, and 1247B are CWL holes and Holes 1244D, 1245A, and 1247A are LWD holes).

Because the density-derived porosity from CWL was degraded more than that from the LWD logs owing to borehole rugosity, LWD density–derived porosity logs are used in all analyses, assuming a two-component system with a matrix density of 2.65 g/cm³ and a water density of 1.03 g/cm³. Porosity correction due to the presence of gas hydrate is accomplished simultaneously with the estimation of gas hydrate saturations (Lee and Collett, 1999).

Clay volume content is calculated from the gamma log using the formula pertinent to tertiary clastic with G_{cn} = 20 (API units) and G_{sh} = 120 (API units), where G_{cn} and G_{sh} are gamma log response in a zone considered clean and log response in a shale bed (Western Atlas, 1995), respectively. The average clay volume contents for Site 1244 (depth range = 85–226 mbsf), Site 1245 (depth range = 85–294 mbsf), and Site 1247 (depth range = 74–202 mbsf) are 13%, 18%, and 15%, respectively.

Figure F2 shows a relationship between LWD density–derived porosity and depth with several empirical compaction curves. The trends in the measured porosities vs. depth at three sites are similar for depths shallower than 250 mbsf. Abnormal porosities at Site 1244 for depths deeper than 250 mbsf are due to the degraded quality of the density logging data below 250 mbsf. Observed compaction trends lie between the compaction curve for shale, derived by Baldwin and Butler (1985), and the compaction curve for terrigenous marine sediments, derived by Hamilton (1976). Compaction curves by Sclater and Christie (1980) for sand and shale are approximately lower and upper limits of observed compaction trends.

The velocity ratio, V_P/V_S, with respect to the LWD density–derived porosity is shown in Figure F3. Figure F3A shows the measured velocity ratios for entire logged intervals and Figure F3B shows measured ratios only for gas hydrate intervals, as interpreted by Collett et al. (this volume). At each well, two distinct modes of velocity ratios with respect to

F2. Porosity and depth, p. 17.
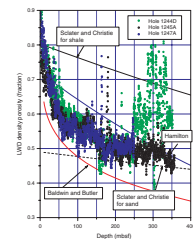
F3. Measured P- and S-wave velocity ratios plotted against density-derived porosity with predicted velocity ratios calculated with various BGTL parameters, p. 18.
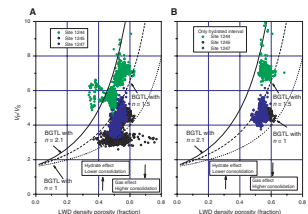
porosity are indicated. For a given density-derived porosity, velocity ratios within the gas hydrate interval (Fig. F3B) are higher than those outside the interval for all wells, indicating either the effect of free gas in sediments on elastic velocities or the difference in the degree of consolidation. Also at a given porosity, velocity ratios at Site 1244 are higher than those at Sites 1245 and 1247, indicating that the degree of consolidation is less at Site 1244. This implies that the BGTL parameter n or m for Site 1244 is different from those for Sites 1245 and 1247. As indicated in Figure F3B, the exponent n appropriate for gas hydrated sediments at Site 1244 is between $n = 1.5$ and $n = 2.1$, whereas it is between $n = 1$ and $n = 1.5$ for Sites 1245 and 1247.

In summary, the following observations can be made for density and velocity logs (only CWL logs are used in this analysis):

1. LWD density–derived porosity generally follows the compaction curve and shows limited scattering in the LWD-derived porosities in the gas-hydrate-bearing interval (shallower than ~130 mbsf), suggesting that the density log–derived porosities are of high quality.
2. Each well log shows two distinct groups of Poisson's (and V_P/V_S) ratios: one for the upper sedimentary section, affected by gas hydrate, and the other for the lower sediment section, affected only by free gas. The decrease of Poisson's ratio at each well from the upper to the lower section is caused partially by compaction and partially by the effect of free gas on velocities.
3. For a given porosity, the V_P/V_S ratio at Site 1244 is highest, whereas the lowest ratio occurs at Site 1245; this implies that the BGTL parameter, m, is lowest at Site 1244 and highest at Site 1245, which in turn implies that sediments at Site 1244 are less consolidated than those at Site 1245.

BASELINE CONDITIONS

In order to estimate the amount of gas hydrate or free gas in sediments, elastic parameters for sediments without gas hydrate or free gas are required; these parameters serve as baseline conditions (no gas or gas hydrate in pore space) for estimating hydrocarbon saturations. One interesting aspect of CWL velocity logs is that the measured V_P is much lower than the velocities anticipated for gas-hydrate-bearing sediments, particularly for Sites 1245 and 1247. It is speculated that the low V_P is indicative of free gas in the sediment, which is either the free gas naturally coexisting with gas hydrate in the GHSZ or gas that has been dissociated from gas hydrate during drilling. If the amount of free gas is small, the effect on V_S is negligible. Therefore, in the case that a small amount of free gas exists in sediments, V_S is more appropriate to derive the baseline conditions for non-gas-hydrate-bearing sediments.

Figure F4 shows the velocities measured below the GHSZ at each site with modeled velocities using the BGTL. S-wave velocity predicted from the BGTL with $m = 2$, $p = 2$ MPa, and $C_v = 0.2$ (solid line) follows the average trend of the measured S-wave velocities at Site 1245 (open circles). For velocities at Site 1244, the BGTL with $m = 1.3$ (dashed line) matches well with the measured S-wave velocities (green dots). The BGTL with $m = 1.8$ (not shown) is optimal for velocities at Site 1247. However, corresponding P-wave velocities predicted from the BGTL indicate that pre-

F4. Measured P- and S-wave velocities with respect to density-derived porosity with predicted velocities from the BGTL (baseline curves), p. 19.
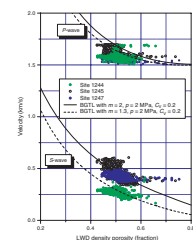
dicted *P*-wave velocities are higher than observed *P*-wave velocities, implying the presence of free gas in sediments.

Therefore, $m = 1.3$, $m = 2$, and $m = 1.8$ are used for the BGTL parameters at Sites 1244, 1245, and 1247, respectively.

Figure F5 shows electrical resistivity vs. LWD density-derived porosities for all measured depths for the three boreholes. The resistivity of formation (R_t) is given by the Archie relation

$$R_t = aR_w\phi^{-j}, \tag{12}$$

where

a, *j* = Archie parameters, and
R_w = the resistivity of connate water.

The baseline resistivities for all three boreholes are interpreted based on the trend of resistivity increase with respect to porosity decrease and are given by

$$R_t = 0.55\phi^{-1.3} \tag{13}$$

The exponent 1.3 is less than the Humble relationship (where the exponent = 2.15), but it is in the low end of the range of cementation factor shown by Jackson et al. (1978). The Archie parameter a and the resistivity of connate water (R_w) is absorbed in the apparent resistivity

$$R_a \ (R_a = aR_w), \tag{14}$$

and $R_a = 0.55$ Ω·m is used for all the analysis of resistivity logs.

ESTIMATION OF GAS HYDRATE AND FREE GAS SATURATIONS

The amount of gas hydrate is estimated from *S*-wave velocities because *P*-wave velocities are more affected by free gas. In order to accurately predict *S*-wave velocities and to estimate saturations of gas hydrate, the BGTL with a depth-dependent exponent *n* (using depth-dependent differential pressure under normal hydraulic pressure), a depth-dependent *G* (using clay volume content and estimated C_h), and parameters shown in Table T1 are used. Saturations of gas hydrate are also estimated from electrical resistivity logs using the Archie relationship.

Figure F6 shows the estimated gas hydrate saturations from *S*-wave velocities (solid curve) and from the resistivity logs (dotted curve) within the GHSZ. The general trend and the magnitude of gas hydrate amount estimated from both *S*-wave velocity and resistivity logs are comparable. The average saturations of gas hydrate estimated from *S*-wave velocities are 10.2%, 10.4%, and 6.1% at Sites 1244, 1245, and 1247, respectively; those estimated form resistivities are 6.5%, 7.9%, and 4.5%, respectively (Table T2). Estimates from velocities are higher than those from resistivities. The largest discrepancy occurs at Site 1244, where the average gas hydrate estimated from *S*-wave velocity is >50% higher than that estimated from the resistivity logging data.

F5. Measured electrical resistivity, p. 20.
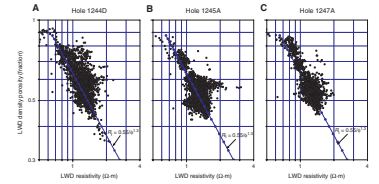
T1. Elastic constants, p. 24.

F6. Gas hydrate saturations estimated from the *S*-wave velocity, p. 21.
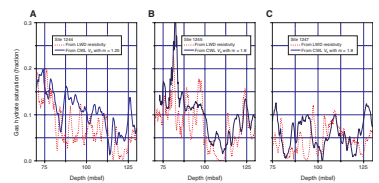
T2. Estimated saturation of gas hydrate and free gas, p. 25.

The amount of free gas can be estimated from two different methods using elastic velocities. The first method applies the BGT with parameters estimated from the BGTL to the *P*-wave velocity, as indicated in Lee (2004). The second method estimates free gas directly from the elastic moduli of sediments.

Because the shallower sedimentary sections on Hydrate Ridge contain gas hydrates, the effect of gas hydrate on *P*-wave velocity needs to be accounted for in the estimation of free gas. This is accomplished by incorporating the amount of gas hydrate estimated from *S*-wave velocity into the *P*-wave velocity model. Figure F7 shows the estimated free gas as solid curves, whereas Table T2 contains the statistics of the estimated free gas saturations. The average saturations of free gas, assuming a patchy distribution with $e = 8$ (equation 11), are estimated to be 0.6%, 1.4%, and 1.5% for Sites 1244, 1245, and 1247, respectively. The above free gas estimations are based on the *P*-wave velocity only. However, if both V_P and V_S are available, the amount of free gas can be estimated directly from the moduli of the sediments (Brie et al., 1995; Murphy et al., 1993). From equations 1 and 8, the Biot coefficient for partially gas-saturated sediments can be written as follows:

$$\beta_{bgt} = 1 - (\mu_{bgtl}/\mu_{ma}) = 1 - (\rho V_S^2/\mu_{ma}), \qquad (15)$$

where

V_S = observed *S*-wave velocity, and
ρ = observed density.

From equation 3, the bulk modulus of formation can be written as

$$k = \rho(V_P^2 - 4V_S^2/3) = k_{ma}(1 - \beta_{bgt}) + \beta_{bgt}^2 M. \qquad (16)$$

From equations 15 and 16, *M* can be calculated; gas saturations can be calculated from *M* and equation 9.

Figure F7 also shows free gas saturations estimated from elastic moduli; these are displayed as dotted curves. Because the effect of gas hydrate is not accounted for in this analysis, we can only compare the estimated free gas saturations below the GHSZ; within this interval the two methods yield similar estimates of gas saturations.

DISCUSSION

Coexistence of Free Gas and Gas Hydrate

As mentioned previously, *P*-wave velocities within the GHSZ at all three sites, particularly at Sites 1245 and 1247, are much lower than normal velocities for water-saturated sediments, whereas the measured *S*-wave velocities are a little higher than those for water-saturated sediments. Low *P*-wave velocities coupled with slightly higher *S*-wave velocities are speculated to be caused by the existence of free gas commingled with gas hydrate. Figures F6 and F7 indicate that the amount of free gas within the GHSZ is approximately proportional to the amount of gas hydrate and is almost continuous throughout the zone.

Several studies have shown that it is possible for free gas and gas hydrate to coexist inside the GHSZ, as discussed below:

F7. Estimated saturations of free gas using the BGT, p. 22.
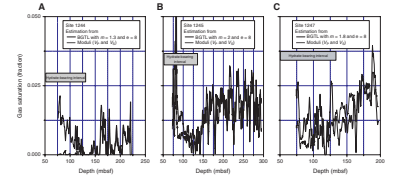
1. Lee and Collett (unpubl. data) demonstrated that there exist free gas zones within the GHSZ at the Cirque-2 well, Alaska (USA), as evidenced by the lack of pore water needed to form gas hydrate. It is known that to form gas hydrate, not only gas but also water is needed. One characteristic of this phenomenon is that these free gas zones are isolated from gas-hydrate-bearing sediments and appear as isolated occurrences of free gas. Somewhat continuous distribution of free gas in this study area may exclude the lack of water as a dominant cause of free gas within the GHSZ.

2. Guerin et al. (1999) showed that gas hydrate and free gas coexist at Site 995 of ODP Leg 164 below the BSR. Ruppel (1997) and Hovland et al. (1997) reported a difference between the depth of the BSR and the theoretical bottom of the GHSZ. They associated this discrepancy with capillary forces developed in fine-grained sediments, which reduce the temperature where gas hydrates dissociate. Gas hydrate grows preferentially in large pore spaces and, reciprocally, dissociates first in smaller pores with strong capillary effects (Hovland et al., 1997). Guerin et al. (1999) speculated that in the interval between the BSR and the GHSZ, gas hydrate within smaller pores may have dissociated and released free gas, while gas hydrate remains present within the larger pores. Therefore, two phases would then coexist in this interval between the BSR and the bottom of the GHSZ. However, this study differs from the results presented here for Leg 204, where free gas exists throughout the GHSZ.

3. Near Site 1250, a double BSR is observed. Double BSRs are often associated with changes in the GHSZ over time caused by seafloor deposition or erosion, sea level fluctuation, local variation in geothermal state, or differences in gas chemistry. The true nature of a double BSRs at this site is not known at this time, but its presence suggests that gas hydrate and free gas may coexist between the BSRs. Nevertheless, a double BSR cannot explain the coexistence free gas and gas hydrate throughout the GHSZ.

4. Sometimes drilling induces the dissociation of gas hydrate near the borehole and releases free gas (Collett et al., 1999). If this is the case, the amount of free gas recorded during or after drilling may be proportional to the amount of gas hydrate in sediments. Free gas would temporarily coexist with gas hydrate in close proximity to the borehole. This is one possible explanation for the presence of free gas within the GHSZ observed at these sites.

5. Vigorous streams of methane bubbles have been observed emanating from vents or the seafloor in southern summit region (Heeschen et al., 2003). The presence of methane bubbles beneath and at the seafloor suggest rapid transport of methane through the GHSZ along faults or fractures. Gorman et al. (2002) showed that the migration of methane gas through the GHSZ in a low-flux hydrate province is also possible (e.g., at the Blake Ridge). The presence of BSRs coupled with the proximity to the summit region means that free gas may migrate through the GHSZ along faults or fractures at these sites. Therefore, it is likely that free gas coexists with gas hydrate within the GHSZ in dynamic systems.

Based on the above arguments, it is probable that gas hydrate coexists with free gas either released by the dissociation of gas hydrate during drilling and/or transported along the fractures and faults.

Amounts of Gas Hydrate

As indicated in Table T2, the average gas hydrate saturations from *S*-wave velocities are 10.2% ± 3.7%, 10.4% ± 5.6%, and 6% ± 3.29% for Sites 1244, 1245, and 1247, respectively. The amounts of gas hydrate estimated from *S*-wave velocities in three holes are higher than those estimated from resistivities. The average saturation of 10% from the *S*-wave velocity at Site 1244 is ~50% higher than that from the resistivity log. The gas hydrate saturation estimated at Site 1244 using the chloride anomaly is between 2% and 8% (Shipboard Scientific Party, 2003), which is close to the estimate from resistivity. At Site 1245, low chloride saturation anomalies are interpreted to reflect in situ hydrate saturations below 3%, with one anomaly suggesting a saturation of 15%. It appears that the estimated gas hydrate saturations from *S*-wave velocities are higher than those from resistivities or chloride anomalies at these sites.

The difference between estimates from *S*-wave velocity and those from the resistivity comes from many factors, such as

1. The locations of LWD wells and CWL wells are not identical. For example, at Site 1247, the holes are ~75 m apart. If the gas hydrate saturations are heterogeneous, there may be some difference between estimates, but it is unlikely that all three wells have higher saturations from *S*-wave velocities.
2. The depth of investigation for CWL *S*-wave velocity and the LWD resistivity may be different. If drilling caused the dissociation of gas hydrate, the effect of dissociation would be more pronounced near the borehole, at the shallow depth of investigation.
3. The assumed parameter, *m*, for the BGTL is lower than it should be. This implies that the degree of consolidation at each well site is underestimated. Therefore, the gas hydrate saturations could have been overestimated. Even though the estimates from *S*-wave velocities are higher than those from resistivities, a similar variation of gas hydrate saturations with depth (Figure F6) suggests that the estimates are reasonable.

Moduli Method vs. BGT with V_P

Figure F7 and Table T2 indicate that free gas saturations estimated below the GHSZ from *P*-wave velocity using the BGT or from both *P*-wave and *S*-wave velocities using the moduli method are similar. The actual amounts of free gas are dependent on the mode of gas distribution or the calibration constant e. Therefore, it is not possible to determine the accuracy of the estimated saturations depicted in Figure F7 and Table T2. However, Figure F7 with Table T2 enables us to examine the accuracy of each method under the same assumptions of gas distribution.

The BGT method with *P*-wave velocity computes the bulk modulus of sediments using the general Biot coefficient shown in equation 7 by incorporating the effect of differential pressure and consolidation or local conditions of sediments through the BGTL parameter *n*. On the other hand, the moduli method calculates the bulk modulus of sediment directly from the measured *P*- and *S*-wave velocities. Therefore, the moduli method is more accurate and reflects better in situ properties of sediments. A good agreement of saturations estimated from the

two methods suggests that (1) the BGTL parameters used in this study are accurate and (2) the theory based on the BGT with parameters derived from the BGTL can be used to predict elastic velocities for partially gas-saturated sediments. Therefore, if both V_P and V_S are available for the estimation of gas saturations, the moduli method is preferable. However, in the case that only V_P is available for an analysis, the BGT based on the BGTL is a viable approach.

Mode of Gas Distribution and Amounts of Free Gas

The amounts of free gas estimated from the *P*-wave velocity data depend on saturation or distribution model of the free gas in the pore space as well as the magnitude of velocity reduction. As shown in equation 9, the calibration constant controls the estimated free gas saturations. Lee (2004) indicates that an appropriate gas saturation model for partially saturated unconsolidated sediments is e = 8, based on the data by Domenico (1977). However, it is difficult to assess the accuracy of the calibration constant without other independent estimations of free gas, because e depends on the frequency (Gei and Carcione, 2003) as well as microstructure of the formation (Murphy et al., 1993). Usually, as the frequency of measurements increases, e decreases, but the precise relation depends on the data.

The dotted line in Figure F8 shows the saturations of the free gas estimated from NMR and density porosities using the method of Freedman (1997). Comparing the free gas estimated shown in Figure F7, the free gas estimations from the NMR technique are about four times greater than free gas saturations estimated from velocities. Note that the comparisons are not valid in the gas-hydrate-bearing intervals because the effect of gas hydrate is not included in the estimation of free gas using the moduli method. As indicated in Figure F8, the general trends of free gas with respect to depth are similar to each other but the details are different.

The saturations of free gas estimated from the NMR technique are independent of the mode of gas distribution in the pore space. Therefore, if the NMR and density porosities are accurate, the dotted line in Figure F8 can be used as a ground truth of free gas saturations. The solid line in Figure F8 is the amount of free gas saturations estimated using the moduli method with e = 2 instead of e = 8, as used in Figure F7. The gas saturations using the moduli method with e = 2 is similar to those from NMR and density porosities. If e = 2 instead of e = 8 is appropriate at these borehole sites, the average free gas saturations estimated from the elastic velocities or the moduli are about four times that of those shown in Table T2. However, the amounts of free gas have not been independently confirmed at these sites. Without any additional data to constrain the amounts of free gas at these sites, it is reasonable to say that estimations using e = 2 and e = 8 correspond to upper and lower limits, respectively.

SUMMARY AND CONCLUSIONS

Based on the physical properties of sediments, such as elastic velocities and electrical resistivity, the amounts of gas hydrate and free gas are estimated from downhole logs at Sites 1244, 1245, and 1247 of ODP Leg 204. In order to accurately estimate the amount of gas hydrate, *S*-wave velocities, not *P*-wave velocities, are used with the BGTL. This is

F8. Estimated saturations of free gas, Site 1245, p. 23.
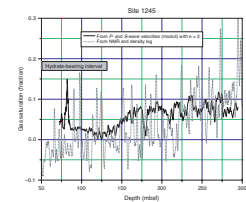
done because *P*-wave velocities are more strongly affected by the gas-hydrate-bearing sediments that are commingled with free gas within the gas hydrate stability zone, possibly owing to the dissociation of gas hydrate during drilling or the migration of free gas through the GHSZ. The amounts of free gas are estimated from *P*-wave velocities using the BGT with parameters derived from the BGTL and are comparable to those estimated from elastic moduli of sediments. However, the amounts of estimated free gas have a high degree of uncertainty, because the calibration constant e is not well constrained and there is no available independent measurements of free gas amounts. This study shows that:

1. At Site 1244, the average gas hydrate saturation within the GHSZ is 10% from *S*-wave velocities, whereas it is 6.5% from electrical resistivities. If the calibration constant of e = 8 is appropriate, average saturations of free gas between 127 and 226 mbsf are negligible (0.4% and 0.3%, based on V_P and moduli methods, respectively). However, the free gas estimates are 1.6% and 1.2% if e = 2 is used, which is comparable to that estimated from the NMR log.
2. At Site 1245, the average gas hydrate saturation within the GHSZ is 10% from *S*-wave velocities, whereas it is 7.9% from electrical resistivity logs. Average saturations of free gas between 129 and 294 mbsf are 1.6% and 1.7%, based on V_P and the moduli methods with e = 8, respectively. However, the free gas estimates are ~6.4% and 6.8% if e = 2 is used.
3. At Site 1247, the average gas hydrate saturation within the GHSZ is 6% from *S*-wave velocities, whereas it is 4.5% from electrical resistivity logs. Average saturations of free gas between 129 and 197 mbsf are 1.7% and 2%, based on V_P and moduli methods with e = 8, respectively. However, the free gas estimates are ~6.8% and 8% if e = 2 is used.

ACKNOWLEDGMENTS

REFERENCES

Baldwin, B., and Butler, C.O., 1985. Compaction curves. *AAPG Bull.,* 69:622–626.

Brie, A., Schlumberger, K.K., Pampuri, F., Marsala, A.F., and Meazza, O., 1995. Shear sonic interpretation in gas-bearing sands [paper presented at Society of Petroleum Engineers Annual Technical Conference and Exhibition, Dallas, TX, 22–25 October 1995], 30595.

Collett, T.S., Lewis, R.E., Dallimore, S.R., Lee, M.W., Mroz, T.H., and Uchida, T., 1999. Detailed evaluation of gas hydrate reservoir properties using JAPEX/JNOC/GSC Mallik 2L-38 gas hydrate research well downhole well-log displays. *In* Dallimore, S.R., Uchida, T., and Collett, T.S. (Eds.), *Scientific Results from JAPEX/JNOC/GSC Mallik 2L-38 Gas Hydrate Research Well, Mackenzie Delta, Northwest Territories, Canada.* Bull.—Geol. Surv. Can., 544:295–311.

Dillon, W.P., Booth, J.S., Paul, C.K., Felhaber, K.L., Hutchinson, D.R., and Swift, B.A., 1991. Mapping of sub-seafloor reservoirs of a greenhouse gas: methane hydrates. *Proc. Int. Symp. Marine Positioning,* 545–554.

Freedman, R., 1997. Gas-corrected porosity from density-porosity and CMR measurements. *In* Allen, D., Crary, S., Freedman, B., Andreani, M., Klopf, W., Badry, R., Flaum, C., Kenyon, B., Kleinberg, R., Gossenberg, P., Horkowitz, J., Logan, D., Singer, J., and White, J. (Eds.), *How to Use Borehole Nuclear Magnetic Resonance.* Oilfield Rev., 9(2):54.

Gei, D., and Carcione, J.M., 2003. Acoustic properties of sediments saturated with gas hydrate, free gas, and water. *Geophys. Prospect.,* 51:141–157.

Gorman, A.R., Holbrook, W.S., Hornbach, M.J., Hackwith, K.L, Lazarralde, D., and Pecher, I., 2002. Migration of methane gas through the hydrate stability zone in a low-flux hydrate province. *Geology,* 30:327–330.

Heeschen, K.U., Tréhu, A.M., and Collier, R.W., 2003. Distribution and height of methane bubble plumes on the Cascadia margin characterized by acoustic imaging. *Geophys. Res. Lett.,* 30:1643–1646.

Jackson, P.D., Taylor-Smith, D., and Stanford, P.N., 1978. Resistivity-porosity-particle shape relationships for marine sands. *Geophysics,* 43(6):1250–1268.

Katzman, R., Holbrook, W.S., and Paull, C.K., 1994. Combined vertical-incidence and wide-angle seismic study of a gas hydrate zone, Blake Ridge. *J. Geophys. Res., [Solid Earth],* 99:17975–17995.

Krief, M., Garta, J., Stellingwerff, J., and Ventre, J., 1990. A petrophysical interpretation using the velocities of *P* and *S* waves (full-waveform sonic). *Log Anal.,* 31:355–369.

Lee, M.W., 2002. Biot-Gassmann theory for velocities of gas-hydrate-bearing sediments. *Geophysics,* 66:763–771.

Lee, M.W., 2003. Elastic properties of overpressured and unconsolidated sediments. *U.S. Geol. Surv. Bull.,* 2214.

Lee, M.W., 2004. Elastic velocities of partially gas-saturated unconsolidated sediments. *Mar. Pet. Geol.,* 21:641–650.

Lee, M.W., and Collett, T.S., 1999. Amount of gas hydrate estimated from compressional- and shear-wave velocities at the JAPEX/JNOC/GSC Mallik 2L-38 gas hydrate research well. *In* Dallimore, S.R., Uchida, T., and Collett, T.S. (Eds.), *Scientific Results from JAPEX/JNOC/GSC Mallik 2L-38 Gas Hydrate Research Well, Mackenzie Delta, Northwest Territories, Canada.* Bull.—Geol. Surv. Can., 544:312–322.

Lee, M.W., and Collett, T.S., in press. Assessment of gas hydrate saturations estimated from sonic logs in the Mallik 5L-38 well, Canada. *In* Dallimore, S.R., and Collett, T.S. (Eds.), *Scientific Results from Mallik 2000 Gas Hydrate Production Research Well Program, Mackenzie Delta, Northwest Territories, Canada.* Bull.—Geol. Surv. Can., 585.

MacKay, M.E., Jarrard, R.D., Westbrook, G.K., Hyndman, R.D., and the Shipboard Scientific Party of ODP Leg 146, 1994. Origin of bottom simulating reflectors: geophysical evidence from the Cascadia accretionary prism. *Geology,* 22:459–462.

Murphy, W., Reischer, A., and Hsu, K., 1993. Modulus decomposition of compressional and shear velocities in sand bodies. *Geophysics,* 58:227–239.

Pecher, I.A., Minshull, T.A., Singh, S.C., and von Huene, R., 1995. Velocity structure of a bottom simulating reflector offshore Peru: result from full waveform inversion. *Earth Planet. Sci. Lett.,* 139:459–469.

Prasad, M., 2002. Acoustic measurements in unconsolidated sands at low effective pressure and overpressure detection. *Geophysics,* 67:405–412.

Shipboard Scientific Party, 2003. Leg 204 summary. *In* Tréhu, A.M, Bohrmann, G., Rack, F.R., Torres, M.E., et al., *Proc. ODP, Init. Repts.,* 204: College Station TX (Ocean Drilling Program), 1–75.

Sloan, E.D., Brewer, P.G., Paull, C.K., Collett, T.S., Dillon, W.P., Holbrook, W.S., and Kvenvolden, K.A., 1999. Future of gas hydrate research. *Eos, Trans. Am. Geophys. Union,* 80:247. (Abstract)

Western Atlas, 1995. *Introduction to Wireline Log Analysis:* Houston, TX (Western Atlas International Inc.).

Figure F1. ODP Leg 204 site location map. Modified from Shipboard Scientific Party (2003).
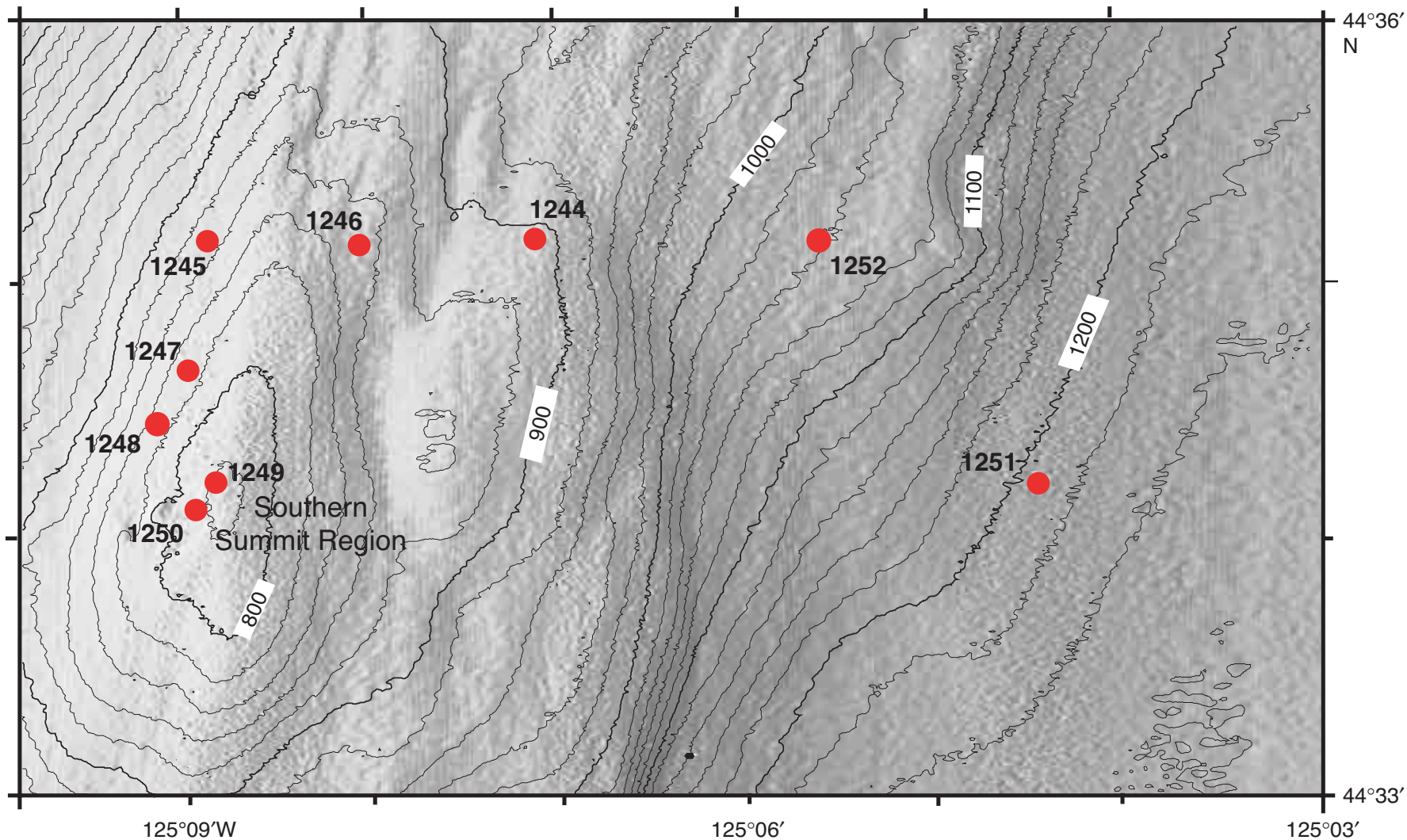
Figure F2. Graph showing the relationship between porosity and depth below seafloor at Sites 1244, 1245, and 1247 of Leg 204 and some empirical compaction curves. Porosity is derived from the logging while drilling (LWD) density log. (Baldwin and Butler [1985] for shale, Sclater and Christie [1980] for sand and shale, and Hamilton [1976] for terrigenous marine sediments.)
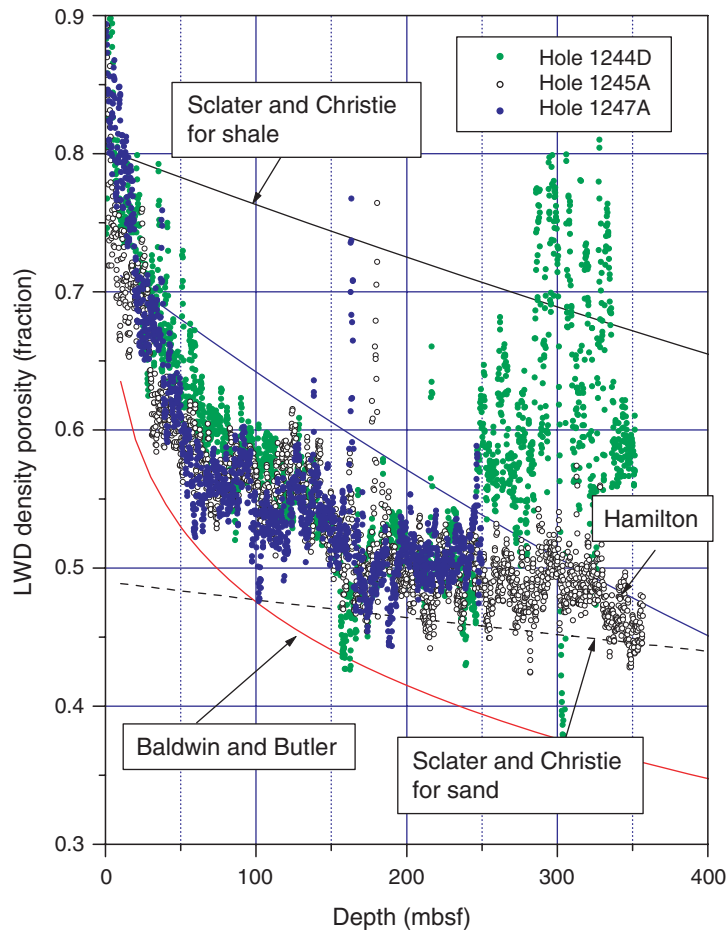
Figure F3. Measured *P*- and *S*-wave velocity ratios plotted against density-derived porosity with predicted velocity ratios calculated with various modified Biot-Gassmann theory by Lee (BGTL) parameters. **A.** All samples. **B.** Samples within the gas hydrate stability zone (gas hydrated interval). LWD = logging while drilling.
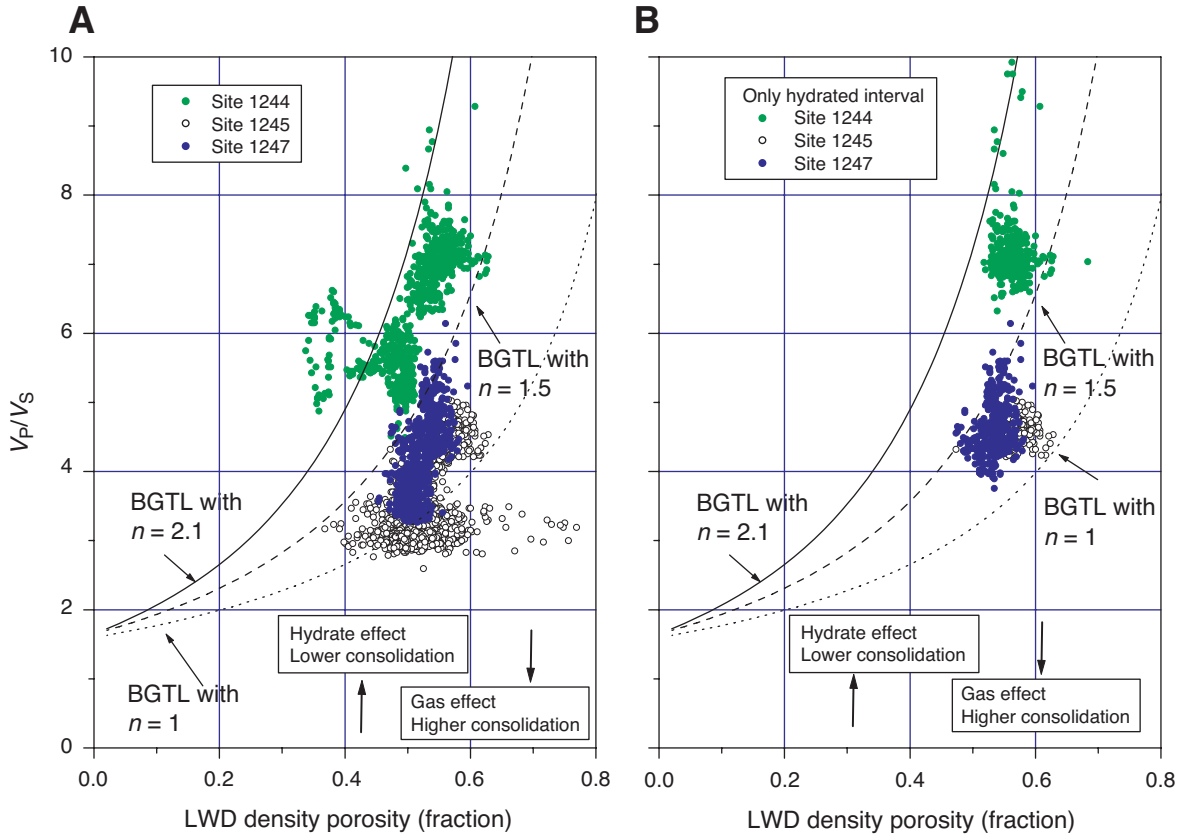
Figure F4. Measured *P*- and *S*-wave velocities with respect to density-derived porosity with predicted velocities from the modified Biot-Gassmann theory by Lee (BGTL) (baseline curves). Measured velocities for Sites 1244, 1245, and 1247 are from depths between 130 and 225, 130 and 295, and 130 and 190 mbsf, respectively. LWD = logging while drilling.
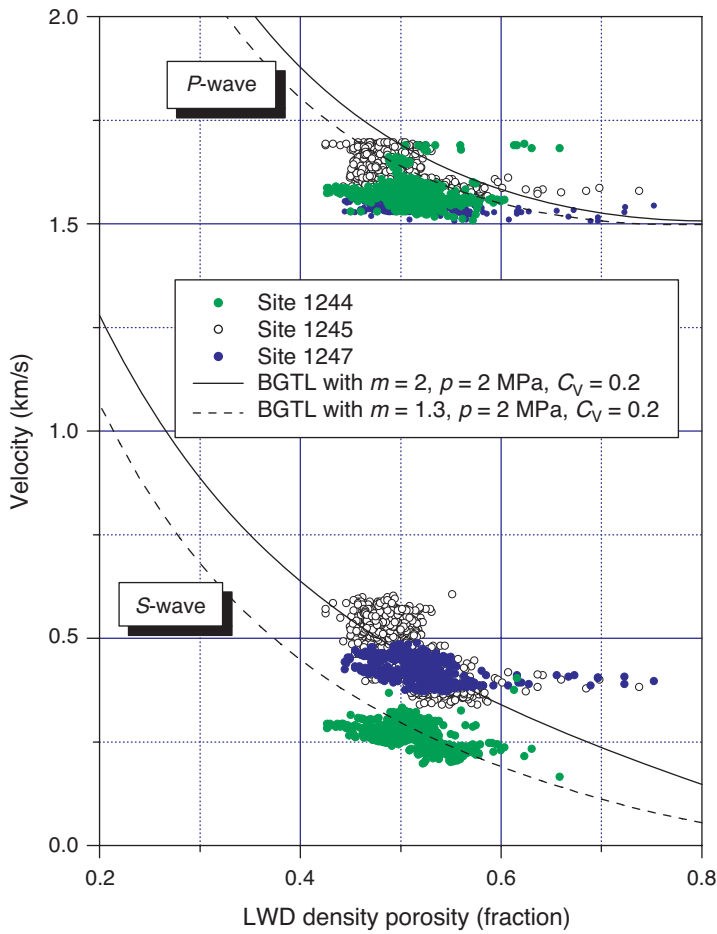
Figure F5. Measured electrical resistivity with respect to LWD density–derived porosity with calculated resistivity using the Archie relation. The depth ranges of measured resistivities for Sites 1244, 1245, and 1247 are between 0.2 and 372, 0.1 and 357, and 0.1 and 250 mbsf, respectively. **A.** Hole 1244D. **B.** Hole 1245A. **C.** Hole 1247A. LWD = logging while drilling.
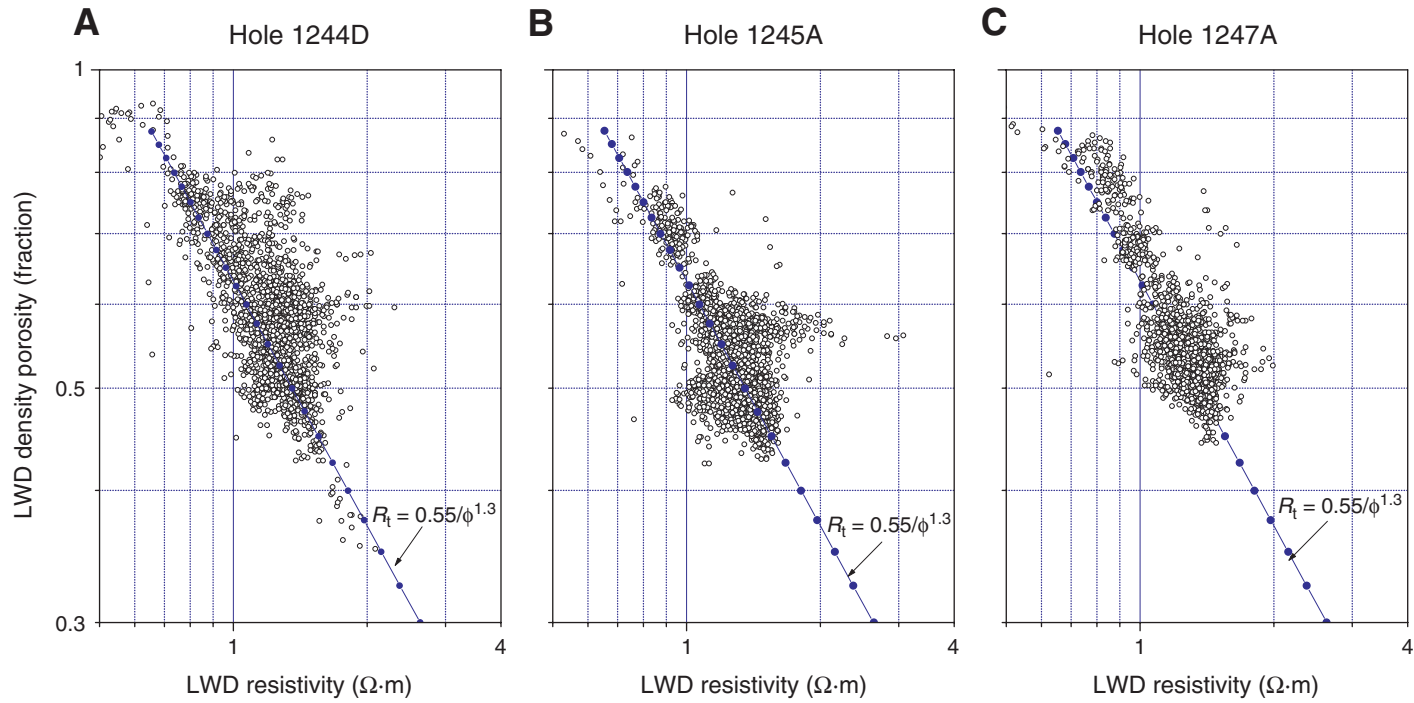
Figure F6. Gas hydrate saturations estimated from the *S*-wave velocity using the BGTL and parameters shown in Table **T1,** p. 24, are denoted as heavy solid lines. Dotted lines represent saturations estimated from electrical resistivity logs. All estimates are smoothed using 11 points (average sampling = 0.15 m). **A.** Site 1244. **B.** Site 1245. **C.** Site 1247. LWD = logging while drilling, CWL = conventional wireline logging.
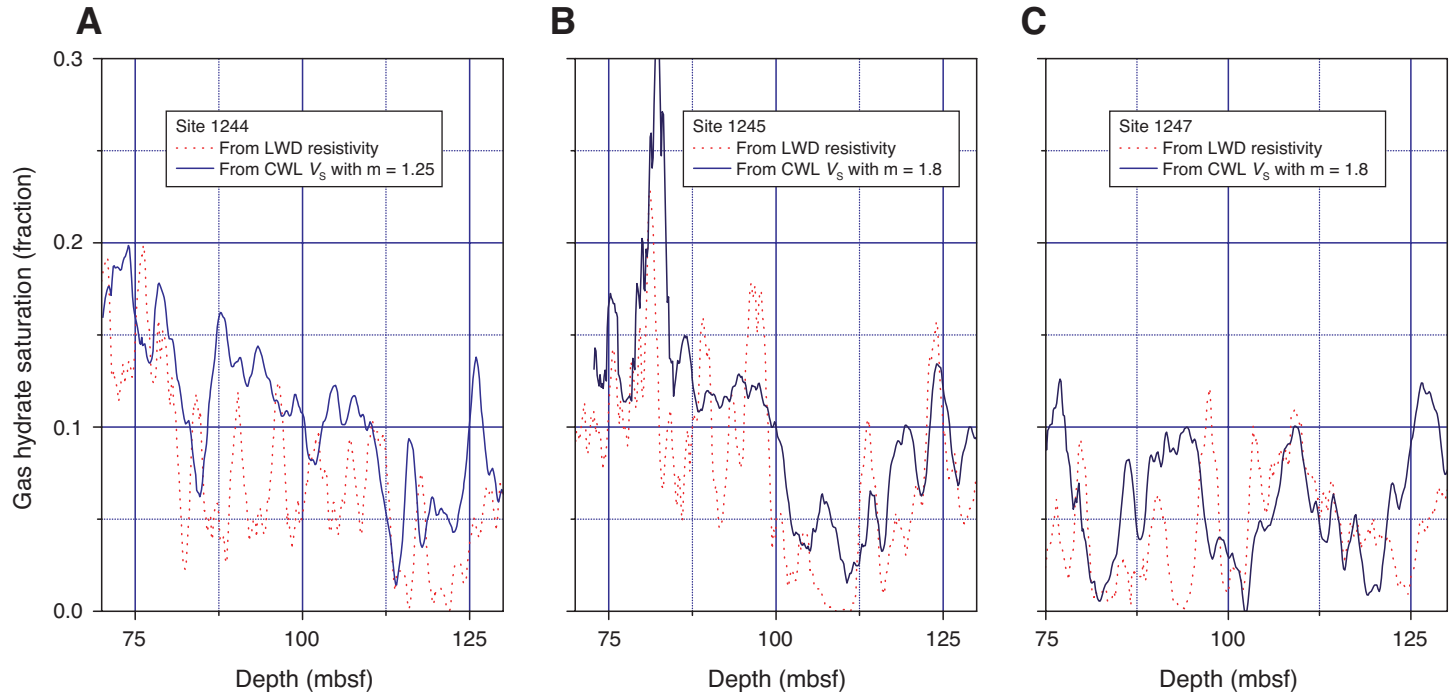
Figure F7. Estimated saturations of free gas using the modified Biot-Gassmann theory by Lee (BGTL) with *P*-wave velocities (solid lines) and those estimated using moduli method with *P*- and *S*-wave velocities (dotted lines) with e = 8. All estimates are smoothed using 11 points (average sampling interval = 0.15 m). **A.** Site 1244. **B.** Site 1245. **C.** Site 1247.
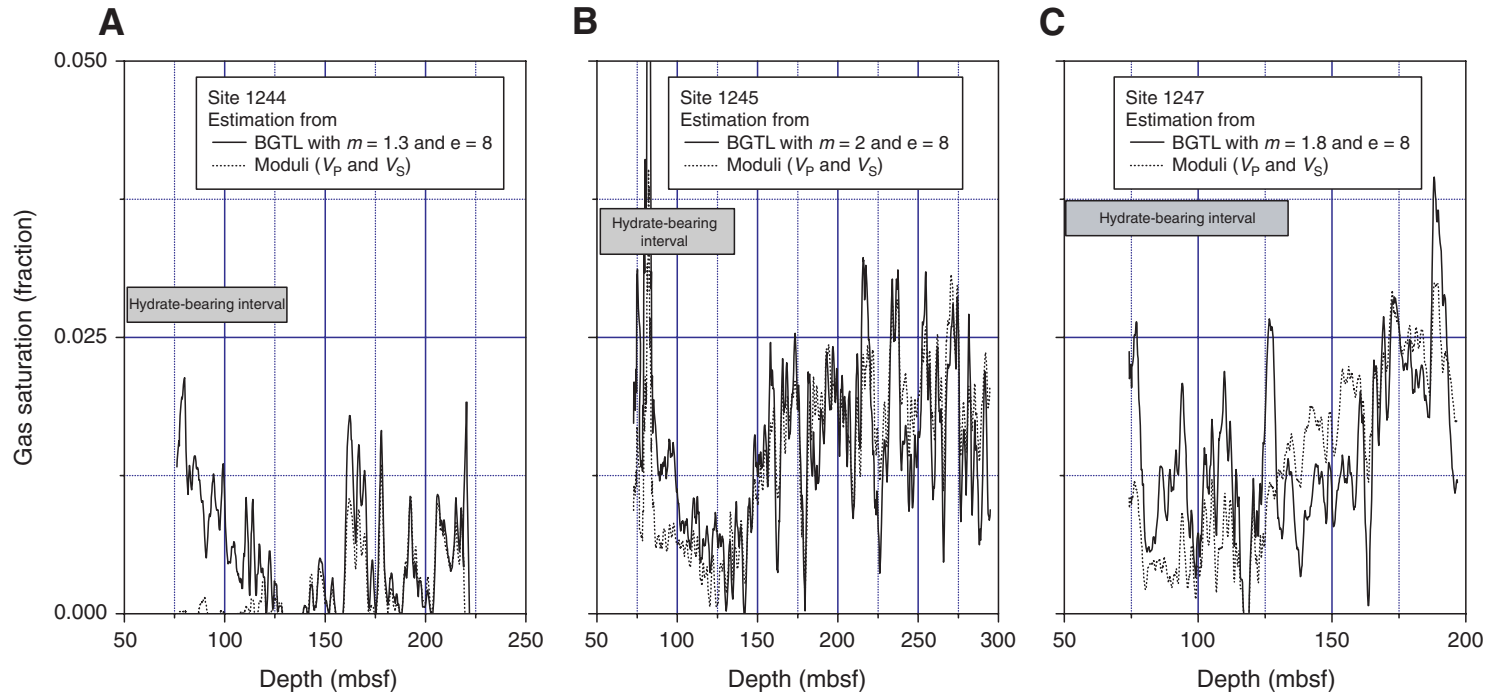
Figure F8. Estimated saturations of free gas at Site 1245. The dotted line represents the estimated free gas from the nuclear magnetic resonance (NMR) and density-derived porosity logs, and the solid line represents the estimated free gas using the moduli method with e = 2. All estimates are smoothed using 11 points (average sampling interval = 0.15 m).
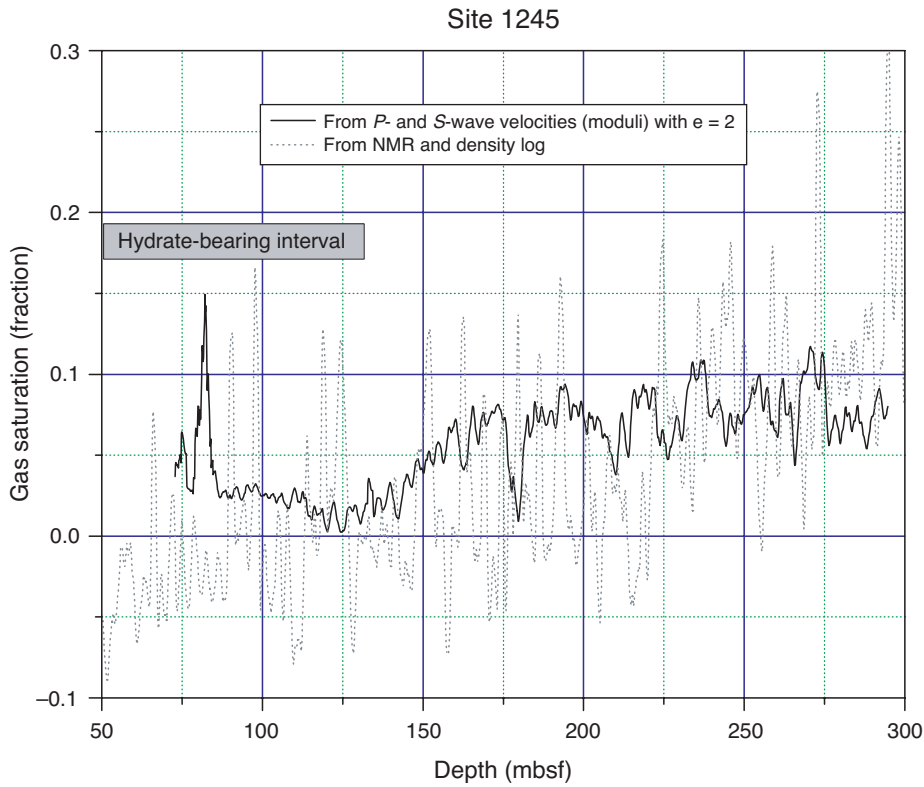

Site 1245

Table T1. Elastic constants.

Elastic constant	Value
Shear modulus of quartz	44 Gpa
Bulk modulus of quartz	38 Gpa
Shear modulus of clay	6.85 Gpa
Bulk modulus of clay	20.9 Gpa
Bulk modulus of water	2.29 Gpa
Bulk modulus of gas	1.11×10^{-4} Gpa
Density of quartz	2.65 g/cm^3
Density of clay	2.58 g/cm^3
Density of water	1 g/cm^3
Density of gas	7.78×10^{-4} g/cm^3

Note: From Lee, 2004.

Table T2. Statistics of estimated saturation of gas hydrate and free gas.

Site	Gas hydrate (C_h) (fraction)	Gas (C_g) (fraction)	Depth (mbsf)	Method
1244	0.102 ± 0.037		76–127	BGTL with V_S
	0.065 ± 0.039		76–127	Archie with resistivity
		0.006 ± 0.005	76–226	BGT with V_P
		0.004 ± 0.005	127–226	BGT with V_P
		0.003 ± 0.003	127–226	Moduli with V_P and V_S
1245	0.104 ± 0.056		73–129	BGTL with V_S
	0.079 ± 0.0550		73–129	Archie with resistivity
		0.016 ± 0.009	73–294	BGT with V_P
		0.016 ± 0.007	129–294	BGT with V_P
		0.017 ± 0.006	74–129	Moduli with V_P and V_S
1247	0.061 ± 0.032		74–129	BGTL using V_S
	0.045 ± 0.028		74–129	Archie with resistivity
		0.015 ± 0.008	74–197	BGT with V_P
		0.017 ± 0.008	129–197	BGT with V_P

Note: BGTL = Modified Biot-Gassmann theory by Lee, BGT = Biot-Gassmann theory.